*33rd EPS Conference on Plasma Phys. Rome, 19 - 23 June 2006 ECA Vol.**30I**, P-1.146 (2006)*

Edge Stability of TCV Plasma

S.Yu.Medvedev[1], A.A.Ivanov[1], A.A.Martynov[1], Yu.Yu.Poshekhonov[1],

R.Behn[2], S.H.Kim[2], J.B.Lister[2], Y.R.Martin[2], O.Sauter[2], L.Villard[2], R.R.Khayrutdinov[3]

[1]*Keldysh Institute, Russian Academy of Sciences, Moscow, Russia*
[2]*CRPP, Association Euratom-Confédération Suisse, EPFL, Lausanne, Switzerland*
[3]*TRINITI, Moscow Region, Russia*

Ideal MHD stability of external kink modes driven by large current density and pressure gradient values in the pedestal region of the tokamak plasma is one of the possible triggers for the edge localized modes (ELM). A number of useful scalings for the edge stability boundaries were derived from the results of the calculations with the KINX code that includes plasma up to the separatrix [1].

Since the ELM triggering mechanism depends on the edge current and pressure profiles, a modification of these parameters can lead to a variation of the ELM cycle controlling their frequency and amplitude as in the magnetic ELM triggering experiments on TCV [2]. Quasi equilibrium modeling of the edge current induction was performed with the adaptive grid free boundary SPIDER code integrated into the DINA-CH Simulink environment. Both edge current generation and plasma boundary shape variations during the vertical oscillation of the plasma were investigated as candidates for the ELM triggering using the KINX code for stability calculations.

A more detailed analysis is required to compare the theoretical scalings with specific experimental observations. TCV can now measure edge profiles more accurately due to an upgrade of the Thomson scattering system [3]. These measurements, with self-consistent equilibria including the edge bootstrap current, are used for quantitative comparisons with experimental observations of ELM characteristics.

1 TCV equilibrium modeling with measured pedestal profiles

The electron temperature and density profiles were obtained for the reproducible shots (TCV-# 26387 to 26393) merging the core and pedestal profiles measurements. The density and temperature profiles were used in the following procedure:

- compute the equilibrium using the reconstructed profiles from LIUQE;
- fix parallel current density profile $j_{||} =< \mathbf{jB} > / < \mathbf{B}\nabla\phi >$, and replace the pressure gradient by the measured $dp/d\psi$ profile.

For all the shots the difference by approximately the same factor 2.3 in poloidal beta β_p values with reconstructed equilibria was encountered. It is not consistent with an estimated 30% increase in the pressure due to ions in typical TCV shots. Not having enough information about the ion component the electron pressure was rescaled to get the LIUQE value for the reconstructed equilibrium ($\beta_p = 0.37$ for # 26383). As for modification of the the current density in the pedestal, collisionless bootstrap current density was used there. The calculations of the bootstrap current taking collisions into account [4] show that the bootstrap current density is about 2 times lower compared to the collisionless values.

The quasi-equilibrium modeling of the ELM triggering sequences was performed using SPIDER code integrated into DINA-CH environment. The ion temperature and density were assumed to be equal to the electron ones $T_i = T_e$ and $n_i = n_e$ giving $\beta_p = 0.3$. The pressure profile in terms of normalized toroidal flux was prescribed together with averaged toroidal current density profile from the reconstructed equilibrium.

For the shot #26383 the maximal current density in the pedestal (after bootstrap current density buildup time that is about 2 ms) is close to the reference equilibrium profile due to the bootstrap current added up to the inductive current.

The perturbation amplitudes close to the TCV simulations of magnetic ELM triggering presented in [5] were obtained: the magnetic axis amplitude was about 1.0 cm and edge current density perturbations were about $0.5 \cdot 10^5$ A/m^2 (lower for higher pedestal) that corresponds to about 3% in parallel current density normalized by current density averaged over plasma cross-section $J_{||}/ < J >$. The plasma shape deformation pattern was found to be in the same

phase with the plasma motion as for the ASDEX Upgrade case [6] but with smaller amplitude. It means that the edge current increase during the upward motion is accompanied by the local squareness decrease of the boundary that possibly counteracts the edge current rise with respect to the edge stability.

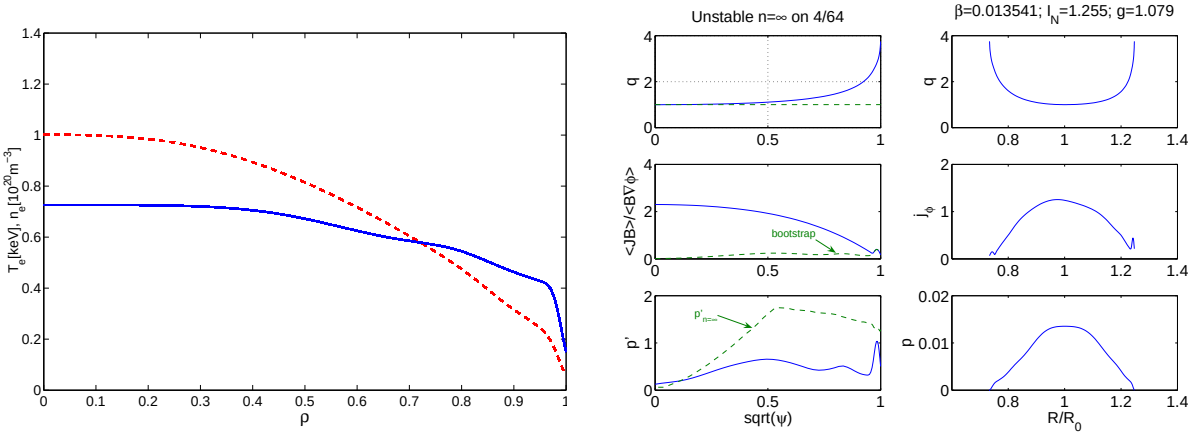

Fig.1.1 The electron temperature (dashed line) and density profiles for the TCV shot #26383 (a). Plasma profiles for the reference equilibrium (b).

2 Plasma shape influence on edge stability

The stability diagrams in the parametric plane $(p'/p'_c, J_{||}/ < J >)$ (where p'_c is the limiting pressure gradient at the plasma edge) were computed using equilibria obtained from the reference one by independently scaling the parallel current density and pressure gradient in the pedestal region. The reference equilibrium edge parameters are shown by green circle in Fig.2.1.

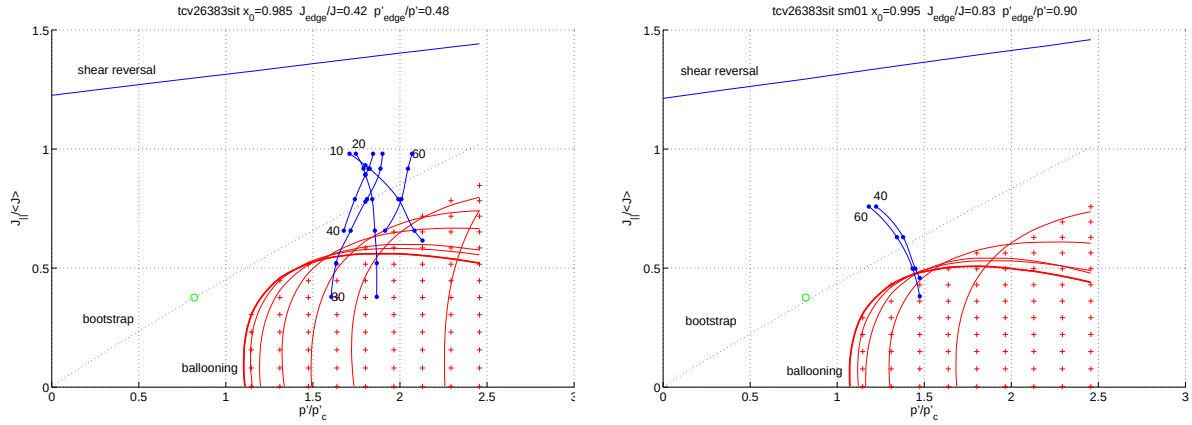

Fig.2.1 Edge stability diagrams for the TCV shot #26383. The profiles for measured (a) and inward-shifted (b) separatrix locations. Toroidal wave numbers for the stability boundaries are given.

In order to simulate an uncertainty in the determination of the separatrix position in the measurements, the pressure profile was cut at $\sqrt{\psi} = 0.99$ (separatrix shifted inside plasma) to get the equilibrium with much larger current density at the edge. As a result, the stability limits were shifted closer to the reference equilibrium. Higher toroidal wave numbers of the external kink/ballooning modes setting the limits can also be observed (Fig.2.1b).

The simulation of the magnetic ELM triggering in ASDEX Upgrade [6] suggested the plasma shape deformation during the perturbation as a possible trigger for ELM. A systematic study of the plasma shape higher order moment influence on the edge kink/ballooning mode stability

was performed using the KINX code taking into account separatrix. For that purpose the plasma boundary was fitted using the following standard expression:

$$R = R_m + a_m \cos(\theta + \delta \sin\theta - \zeta(\theta)\sin 2\theta), \quad Z = Z_m + a_m E \sin\theta, \quad 0 < |\theta| < \pi.$$

The fitting was performed separately for upper and lower plasma parts (with $Z = Z_m$ defined at the point where $R = \max(R)$. To take into account the difference between outboard ζ_o and inboard ζ_i squareness the function $2\zeta(\theta) = \zeta_o + \zeta_i + (\zeta_o - \zeta_i)\cos\theta$ was chosen. The results of the least square fit give $\delta = 0.34$ and $\zeta_o = 0.05$ for the upper part of the plasma for the shot #26383 at $t = 0.85s$.

The plasma geometry scans were performed in the values of upper triangularity and upper outboard squareness - higher order moments that affect the local plasma cross-section curvature and second stability access near the edge [7]. In Fig. 2.2a the $n = \infty$ ballooning mode stability boundaries at the bootstrap line in the parametric plane are shown under triangularity variation.

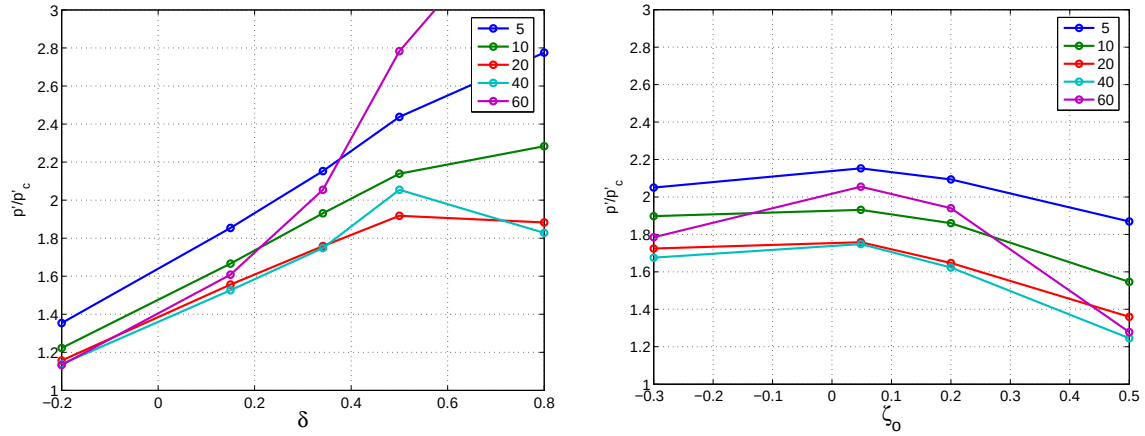

Fig.2.2 The stability limit in p'/p'_c at the bootstrap line under triangularity (a) and squareness (b) variations. Different curves correspond to different toroidal wave numbers.

The squareness scan reveals the optimal value near zero squareness for the fixed reference triangularity (Fig.2.2b). Let us note that both the case of negative triangularity and high positive squareness correspond to $n = \infty$ ballooning mode destabilization at the bootstrap line. This is demonstrated by the behavior of the $n = \infty$ ballooning stability limits in the parametric plane (Fig.2.3).

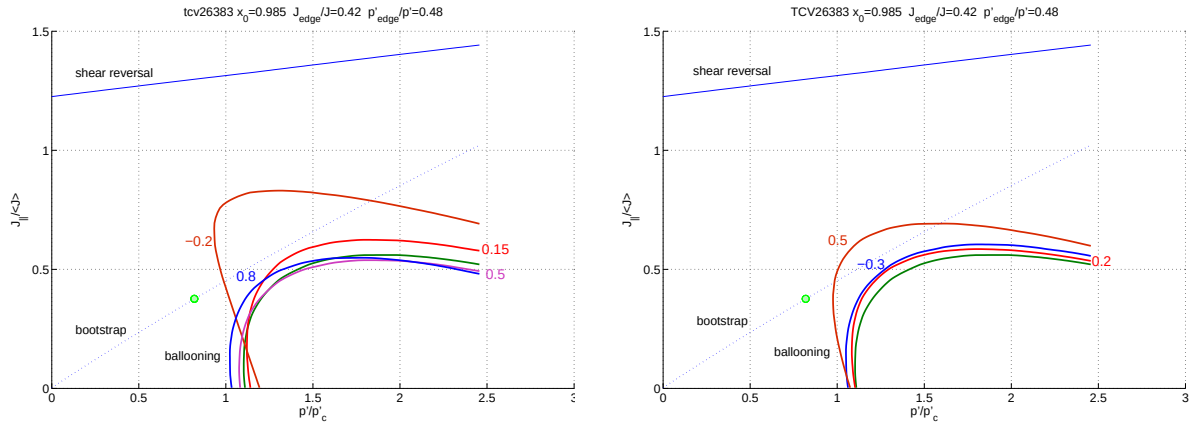

Fig.2.3 The $n = \infty$ stability limits in the parametric plane. The local limit at $\sqrt{\psi} = 0.985$ is shown. Triangularity (a) and squareness (b) variations. Different curves correspond to different values of triangularity and squareness.